



RESEARCH ARTICLE

Inter-subject stability and regional concentration estimates of 3D-FID-MRSI in the human brain at 7 T

Gilbert Hangel^{1,2}  | Benjamin Spurny-Dworak³ | Philipp Lazen¹ |
 Cornelius Cadrien^{1,2} | Sukrit Sharma¹ | Lukas Hingerl¹ | Eva Hečková¹ |
 Bernhard Strasser¹ | Stanislav Motyka¹ | Alexandra Lipka^{1,4} | Stephan Gruber¹ |
 Christoph Brandner⁵ | Rupert Lanzenberger³ | Karl Rössler² |
 Siegfried Trattnig^{1,4} | Wolfgang Bogner¹ 

¹High-field MR Center, Department of Biomedical Imaging and Image-guided Therapy, Medical University of Vienna, Vienna, Austria

²Department of Neurosurgery, Medical University of Vienna, Vienna, Austria

³Division of General Psychiatry, Department of Psychiatry and Psychotherapy, Medical University of Vienna, Vienna, Austria

⁴Institute for Clinical Molecular MRI, Karl Landsteiner Society, St. Pölten, Austria

⁵High-field MR Center, Center for Medical Physics and Biomedical Engineering, Medical University of Vienna, Vienna, Austria

Correspondence

Gilbert Hangel, Medical University of Vienna,
 Department of Neurosurgery and High Field
 MR Centre, Währinger Gürtel 18-20, 1090
 Vienna, Austria.

Email: gilbert.hangel@meduniwien.ac.at

Funding information

Austrian Science Fund (FWF), Grant/Award
 Numbers: P 34198, P 30701, KLI-646

Purpose: Recently, a 3D-concentric ring trajectory (CRT)-based free induction decay (FID)-MRSI sequence was introduced for fast high-resolution metabolic imaging at 7 T. This technique provides metabolic ratio maps of almost the entire brain within clinically feasible scan times, but its robustness has not yet been thoroughly investigated. Therefore, we have assessed quantitative concentration estimates and their variability in healthy volunteers using this approach.

Methods: We acquired whole-brain 3D-CRT-FID-MRSI at 7 T in 15 min with 3.4 mm nominal isometric resolution in 24 volunteers (12 male, 12 female, mean age 27 ± 6 years). Concentration estimate maps were calculated for 15 metabolites using internal water referencing and evaluated in 55 different regions of interest (ROIs) in the brain. Data quality, mean metabolite concentrations, and their inter-subject coefficients of variation (CVs) were compared for all ROIs.

Results: Of 24 datasets, one was excluded due to motion artifacts. The concentrations of total choline, total creatine, glutamate, myo-inositol, and *N*-acetylaspartate in 44 regions were estimated within quality thresholds. Inter-subject CVs (mean over 44 ROIs/minimum/maximum) were 9%/5%/19% for total choline, 10%/6%/20% for total creatine, 11%/7%/24% for glutamate, 10%/6%/19% for myo-inositol, and 9%/6%/19% for *N*-acetylaspartate.

Abbreviations: Asp, aspartate; CRLB, Cramér-Rao lower bound; CRT, concentric ring trajectory; CSF, cerebrospinal fluid; EPSI, echo-planar spectroscopic imaging; FID, free induction decay; FWHM, full width at half maximum; GABA, γ -aminobutyric acid; Gln, glutamine; Glu, glutamate; Gly, glycine; GM, gray matter; GSH, glutathione; mIns, myo-inositol; MRSI, magnetic resonance spectroscopic imaging; NAA, *N*-acetylaspartate; NAAG, *N*-acetylaspartylglutamate; ROI, region of interest; SAR, specific absorption rate; Ser, serine; sIns, scyllo-inositol; SNR, signal-to-noise ratio; SVS, single-voxel spectroscopy; Tau, taurine; tCho, phosphocholine + glycerophosphocholine; tCr, total creatine (creatine + phosphocreatine); T_E , echo time; T_R , repetition time; WET, water suppression enhanced through T_1 effects; WM, white matter.

This is an open access article under the terms of the Creative Commons Attribution License, which permits use, distribution and reproduction in any medium, provided the original work is properly cited.

© 2021 The Authors. *NMR in Biomedicine* published by John Wiley & Sons Ltd.

Discussion: We defined the performance of 3D-CRT-based FID-MRSI for metabolite concentration estimate mapping, showing which metabolites could be robustly quantified in which ROIs with which inter-subject CVs expected. However, the basal brain regions and lesser-signal metabolites in particular remain as a challenge due to susceptibility effects from the proximity to nasal and auditory cavities. Further improvement in quantification and the mitigation of B_0/B_1 -field inhomogeneities will be necessary to achieve reliable whole-brain coverage.

KEYWORDS

7 T, healthy brain, high resolution, inter-subject reproducibility, MRS, MRSI

1 | INTRODUCTION

Proton magnetic resonance spectroscopic imaging (MRSI) in the brain based on the direct acquisition of the free induction decay (FID) signal has been introduced to overcome many technical challenges with ultra-high-field systems.^{1,2} Such challenges include lower B_0/B_1 homogeneity, more restricted specific absorption rate (SAR), and shorter T_2 times.³ This simple acquisition scheme further reduces SAR, eliminates signal loss due to T_2 relaxation and J coupling, improves spatial selection, and enables short repetition times (T_R).^{1,2} Over the last several years, technical improvements have concentrated on faster data acquisition to reach shorter measurement times, increased brain coverage, and higher spatial resolutions, which are attractive for clinical metabolic brain mapping.⁴ Starting with parallel imaging techniques,^{5–8} echo-planar spectroscopic imaging (EPSI),⁹ and T_R reduction,^{10–12} these recent innovations have concentrated on spatial-spectral encoding using spiral,^{13,14} rosette,¹⁵ and concentric ring trajectories (CRTs).^{16–20} Research culminated in a CRT-based 3D-MRSI sequence at 7 T that can cover the whole brain with ~ 3 mm isotropic resolution, acquired in 10–15 min.^{21,22}

7 T MRSI, with an increased signal-to-noise ratio (SNR) and spectral dispersion, compared with lower-field MR scanners, enables imaging of a wide range of metabolites, eg improving the separation of *N*-acetylaspartate (NAA) from *N*-acetylaspartylglutamate (NAAG), glutamate (Glu) from glutamine (Gln), or glycine (Gly) from myo-inositol (mIns).^{22–24} Based on these benefits, 7 T MRSI has been successfully applied to research applications ranging from γ -aminobutyric acid (GABA) mapping^{25,26} to the resolution of metabolism in tumors,^{9,22–24,27} multiple sclerosis,²⁸ and epilepsy.²⁹

While many technical milestones have been reached, open questions remain with respect to the stability of these whole-brain and/or high-resolution MRSI methods. This includes inter-subject variations of metabolite concentrations in different brain regions, as well as intra-subject variations over time. So far, we had only investigated these variations for FID-MRSI in a small study at 3 T.³⁰ Historically, the results of MRSI quantification have varied greatly depending on study design, data evaluation, and investigated brain regions.^{31–37} To facilitate the use of MRSI for clinical and research applications, we have to first establish the normal concentrations of metabolites within different brain regions of healthy volunteers instead of relative signals as previously.

To evaluate the performance and inter-subject stability of our 7 T 3D-CRT-FID-MRSI approach, we conducted a study with a larger subject cohort, detailed quantification estimation and regional evaluation.

1.1 | Purpose

The purpose was to acquire whole-brain, 3D-CRT-based FID-MRSI at 7 T in a wider cohort (24 volunteers) than in our previous volunteer studies and to derive for the first time concentration estimates for our method, and further to assess the local MRSI data quality in an array of different small and large brain regions in order to evaluate the quantification robustness and inter-subject variability for the concentration estimates of individual metabolites.

The results will define the performance limits of our 3D-CRT-based FID-MRSI method at 7 T in regard to which metabolites can be confidently and reliably mapped in which regions of the brain.

2 | EXPERIMENTAL

2.1 | Subject recruitment

This study was conducted with the approval of the local institutional review board. Subjects were included in this study when no contraindications for 7 T MRI (eg claustrophobia, ferromagnetic implants, non-ferromagnetic metal head implants >12 mm, or pregnancy) were

reported. Written and informed consent was obtained from all 24 young healthy volunteers (12 male, 12 female, mean age 27 ± 6 years, Table 1). We chose a young cohort due to expected good compliance for motionlessness and easy reproducibility.

2.2 | 7 T MRSI measurement protocol

We performed the measurement protocol using a 7 T whole-body MR imager (Magnetom, Siemens Healthineers, Erlangen, Germany), located at the High Field MR Centre of the Medical University of Vienna, featuring a gradient system with a 70 mT/m maximum gradient strength per direction and a 200 mT/m/s slew rate as well as a 32-channel head receive coil array (Nova Medical, Wilmington, MA). The protocol included B_1^+ maps for flip-angle optimization, B_0 maps, and magnetization prepared two rapid gradient echoes (MP2RAGE) as the T_1 -weighted morphological MRI reference (T_R 5000 ms, T_E 4.13 ms, T_{11} 700 ms, T_{12} 2700 ms, $0.75 \times 0.75 \times 0.75$ mm³ resolution, 8 min 2 s with GRAPPA factor 3).

Our 3D-CRT-FID-MRSI sequence (a detailed description of sequence design and implementation can be found in Reference²¹) employed in-plane 2D-CRT, and through-plane phase encoding of an ellipsoidal k -space resulted in a $64 \times 64 \times 39$ matrix over a field of view of $220 \times 220 \times 133$ mm³. This corresponds to a nominal spatial resolution of $3.4 \times 3.4 \times 3.4$ mm³ and an effective resolution of $4.7 \times 4.7 \times 4.7$ mm³ or 0.1 cm³. A slab of 110 mm thickness starting at the superior part the brain was selected with slices oriented in parallel to the horns of the corpus callosum. Other MRSI scan parameters included T_R of 450 ms, scan time of 15 min, acquisition delay of 1.3 ms, 39° excitation flip angle (calculated as nominal average Ernst angle of NAA, tCr (creatine + phosphocreatine), tCho (phosphocholine + glycerophosphocholine), Glu, mlins⁵), readout duration of 345 ms, spectral bandwidth of 2778 Hz, variable temporal interleaves (eg 1-3 depending on the respective ring radii to maintain the spectral bandwidth for larger readout circles), and 7 T-optimized WET water suppression.^{10,38} No lipid suppression was employed during acquisition to allow a short T_R . A second MRSI scan, without water suppression, included a T_R of 200 ms, a

TABLE 1 Overview of all volunteer subjects measured in this study. In some volunteers, individual ROIs had to be excluded due to poor segmentation of the GM from the WM

Volunteer	Sex	Age [years]	Regions excluded due to poor GM/WM segmentation
1	Male	24	
2	Male	34	
3	Male	23	
4	Male	23	
5	Female	33	Parietal GM, WM, GM + WM
6	Female	23	
7	Female	24	
8	Female	29	Parietal GM, WM, GM + WM
9	Male	33	Frontal, motor, parietal GM, WM, GM + WM
10	Female	19	
11	Female	21	
12	Female	20	
13	Male	31	
14	Male	23	
15	Male	38	
16	Male	27	
17	Male	35	
18	Male	39	
19	Female	22	
20	Female	23	Parietal GM, WM, GM + WM
21	Female	24	
22	Male	34	
23	Female	23	
24	Female	20	Frontal, motor, parietal GM, WM, GM + WM

readout duration/spectral bandwidth of 158 ms/606 Hz, and an Ernst angle of 27°, but with otherwise identical spatial coverage, and was acquired in 3 min 18 s as an internal water reference. This second scan was necessary as we required an unsuppressed water signal as reference.

2.3 | Data processing and quantification

For offline MRSI processing, we utilized our in-house-developed software pipeline³⁹ that is based on MATLAB (MathWorks, Natick, MA), Bash (Free Software Foundation, Boston, MA), FSL (Analysis Group, FMRIB, Oxford, UK), and MINC (MINC Tools, McConnell Brain Imaging Center, Montreal, QC, Canada). This pipeline included iMUSICAL (interleaved multichannel spectroscopic data combined by matching image calibration data) coil combination based on interleaved water calibration scans,^{17,20} k -space reconstruction with in-plane convolution gridding^{20,40} (weighting non-Cartesian points in relation to the Cartesian target point), off-resonance correction to compensate the time delay of acquisition samples⁴¹ and spatial Hamming filtering, as well as post-measurement lipid signal removal by L2 regularization^{42,43} prior to spectral quantification. Reconstruction did not include eddy current correction, as CRTs are inherently resistant to these.¹⁸ It further did not include B_0 or B_1 correction (while differences in local flip angles can lead to differences in the effective T_1 weighting, we previously found only little impact for FID-MRSI⁴⁴). A graphical overview of the reconstruction pipeline is available in Supporting Figure 1.

Each spectrum was separately quantified via LCMoDel (v6.3-1, LCMODEL, Oakville, Ontario, Canada)⁴⁵ over evaluation ranges of 0.2-1.2 ppm and 1.8-3.88 ppm (excluding the lipid spectral range of 1.2-1.8 ppm due to possible remaining lipid signal after L2 regularization; the upper limit of 3.88 was necessary due to water suppression effects). Our basis set, simulated in NMRscope-B⁴⁶ accounting for the first-order phase caused by the acquisition delay of 1.3 ms, included the following neurochemicals: tCr, tCho, NAA, NAAG, Glu, Gln, mIns, scyllo-inositol (slns), GABA, glutathione (GSH), Gly, taurine (Tau), cysteine, serine (Ser), and aspartate (Asp). An average macromolecular background based on prior studies with metabolite-nulled measurements was included to improve quantification.^{47,48} Water was quantified separately from the unsuppressed reference scan, using LCMoDel as well, with a water basis simulated as above. SNR (using the pseudo-replica method with receiver noise prescans acquired at the start of the MRSI sequence⁶) and full width at half maximum (FWHM) were calculated voxel-wise from the LCMoDel fits of NAA and tCr at 3.02 ppm.

For the calculation of concentration estimates using the internal water concentration as a reference, T_1 -weighted images were segmented into gray matter (GM)/white matter (WM)/cerebrospinal fluid (CSF) using FSL's FAST tool and the segmentations were resampled to the MRSI resolution. Only the GM/WM segmentations were used for further analysis. Molar concentrations of 36.1 mol/L for GM, 43.3 mol/L for WM, and 53.8 mol/L for CSF were assumed based on literature.⁴⁹ The T_1 relaxation times, which are necessary for the correction of saturation effects at short T_R , were taken from the literature or estimated as an average of known T_1 values for metabolites without published human 7 T values (Table 2).^{50,51} Due to the use of an ultra-short acquisition delay of 1.3 ms, we did not deem T_2 corrections necessary. Metabolite concentrations were estimated as previously described^{52,53}: in short, for every MRSI voxel, tissue segmentation was used to calculate T_1 correction factors for all metabolites and water, according to the GM and WM content, and applied to the signal derived from the LCMoDel fitting results. Concentration

TABLE 2 T_1 times for metabolites and water for GM and WM used for concentration estimates in this study. Lacking reported literature values for human in vivo MRS at 7 T, we used an average of known 7 T T_1 times (ie NAA, tCr, tCho, mIns, Glu, Gln, GSH, Tau, NAAG) for Gly and Ser

Compound	T_1 GM [ms]	T_1 WM [ms]	Reference
Asp	1000	1000	Estimated from ⁵¹
tCho	1510	1320	50
tCr 3 ppm	1780	1740	50
GABA	1100	1200	94
Glu	1610	1750	50
Gln	1540	1740	50
Gly	1400	1400	Average estimate from known compounds
GSH	1140	1060	50
mIns	1280	1190	50
NAA	1535	1545	, ⁵⁰ average of resonances
NAAG	1210	940	50
Ser	1400	1400	Average estimate from known compounds
Tau	2150	2090	50
Water	2000	1550	50

TABLE 3 Evaluation of region fitting quality, including rejected regions. ROIs were separated based on the percentage of voxels that fulfilled the criteria of all of NAA, tCr, tCho, and mIns with CRLBs < 40%. Further listed is the estimated GM/WM content of our segmentations, mean ROI size (for comparison, effective voxel size = 0.1 cm³) as well as the percentage of voxels for a metabolite in an ROI that had a CRLB of <20% for NAA, tCr, tCho, and Ins, and <40% for all others

ROI > 80%	GM [%]	WM [%]	Mean ROI size [cm ³]	tCho [%]	tCr [%]	GABA [%]	Glu [%]	Gln [%]	Gly [%]	GSH [%]	mIns [%]	NAA [%]	NAAG [%]	Ser [%]	Tau [%]
Subcortical WM (left)	35	63	101.4	85	81	47	83	50	33	46	78	84	59	61	52
Subcortical WM (right)	35	62	101.0	87	84	50	85	52	34	50	82	85	62	62	57
Subcortical WM (bilateral)	35	63	202.4	86	82	48	84	51	33	48	80	85	61	61	54
Motor subcortex WM	31	68	18.4	98	97	74	97	50	54	54	97	98	90	78	78
Motor cortex GM	63	27	18.7	86	83	62	86	55	36	32	81	87	70	67	70
Motor cortex/ subcortex GM + WM	47	47	37.1	92	90	68	92	53	45	43	89	92	80	72	74
Parietal subcortex WM	35	64	47.6	98	97	64	96	60	54	58	96	98	84	78	77
Parietal cortex GM	63	27	66.0	91	89	62	91	66	45	42	87	92	72	71	76
Parietal cortex/ subcortex GM + WM	50	44	103.6	94	93	63	93	63	49	49	91	95	77	74	77
Cingulate subcortex WM	31	69	13.8	91	87	53	88	37	26	64	84	91	64	61	40
Cingulate cortex GM	77	23	11.0	91	89	66	92	60	29	52	85	91	68	68	62
Cingulate cortex/ subcortex GM + WM	51	49	24.9	91	88	59	90	47	27	58	84	91	66	64	50
Visual subcortex WM	33	60	13.6	90	82	29	84	39	33	40	74	89	49	71	56
Primary somatosensory subcortex WM	39	57	7.2	95	93	64	95	61	41	40	93	95	80	74	72
Primary somatosensory cortex/ subcortex GM + WM	49	41	16.8	87	84	57	87	57	36	32	83	88	69	66	67
Thalamus	42	58	7.4	90	84	49	84	37	14	51	75	87	58	53	27
Putamen	55	45	5.1	89	86	39	90	67	11	53	72	87	46	54	32
Non-lobe WM	10	90	31.9	94	91	45	86	34	31	73	86	93	68	61	36
ROI > 66%															
Cortical GM (left)	65	26	124.3	69	63	40	69	48	23	30	59	69	44	50	47
Cortical GM (right)	61	25	123.9	78	74	46	77	55	28	36	71	77	52	55	57
Cortical GM (bilateral)	63	25	248.2	73	69	43	73	52	25	33	65	73	48	52	52
Cortical GM + subcortical WM (left)	51	43	225.7	76	71	43	75	49	27	37	68	76	51	55	49

(Continues)

TABLE 3 (Continued)

ROI > 80%	GM [%]	WM [%]	Mean ROI size [cm ³]	tCho [%]	tCr [%]	GABA [%]	Glu [%]	Gln [%]	Gly [%]	GSH [%]	mIns [%]	NAA [%]	NAAG [%]	Ser [%]	Tau [%]
Cortical GM + subcortical WM (right)	49	43	224.9	82	78	48	81	54	30	42	76	81	57	58	57
Cortical GM + subcortical WM (bilateral)	50	43	443.8	79	75	46	78	51	29	40	72	78	54	56	53
Subcortical GM (left)	51	48	14.8	83	78	35	78	43	11	52	65	78	44	42	25
Subcortical GM (right)	50	50	14.4	77	68	32	68	40	9	45	57	69	32	39	19
Subcortical GM (bilateral)	51	49	29.3	80	73	33	72	41	10	49	61	74	38	40	22
Auditory subcortex WM	43	53	7.0	85	79	39	81	62	19	41	75	79	42	55	42
Auditory cortex GM	62	24	12.2	73	67	35	70	55	15	31	60	68	33	45	41
Auditory cortex/ subcortex GM + WM	54	36	19.2	77	71	36	74	58	16	35	66	72	36	49	41
Occipital subcortex WM	34	61	22.4	86	79	30	80	40	30	39	73	84	45	64	51
Occipital cortex GM	59	28	29.5	75	66	30	73	41	22	28	60	74	40	56	49
Occipital cortex/ subcortex GM + WM	48	43	51.9	80	71	30	76	41	26	33	65	78	42	59	50
Temporal subcortex WM	38	59	33.8	72	67	33	70	50	19	39	64	69	43	47	35
Temporal cortex/ subcortex GM + WM	52	41	77.0	66	60	32	64	49	17	33	56	62	38	44	35
Frontal subcortex WM	34	64	80.8	82	80	50	83	51	28	46	77	82	57	55	50
Frontal cortex GM	62	23	96.4	66	62	41	68	48	17	31	59	67	41	43	44
Frontal cortex/ subcortex GM + WM	49	43	177.2	73	70	45	74	50	22	38	67	74	48	48	47
Visual cortex GM	55	28	17.1	76	65	26	76	39	22	27	58	79	42	61	49
Visual cortex/ subcortex GM + WM	45	43	30.7	82	73	27	80	39	27	33	65	84	45	65	52
Primary somatosensory cortex GM	57	28	9.6	80	77	52	81	55	32	26	75	82	61	60	63
Pallidum	13	87	1.9	81	79	37	75	43	4	53	55	76	32	35	13
Hippocampus	72	26	4.1	81	69	23	65	37	12	51	56	66	27	28	23
Corpus callosum	29	71	1.8	83	73	41	77	25	17	58	68	82	49	48	19
Mean	47	47	67.0	83	78	45	80	49	27	43	73	81	54	57	49

Below quality threshold: brain stem, cerebellum (left, right, bilateral), cerebral WM (left, right, bilateral), amygdala, nucleus accumbens, temporal cortex (GM), ventral diencephalon.

estimates for each spectrum were then calculated as the ratio of metabolite-to-water signal multiplied by the local water concentration and the correction factor calculated before influenced by the respective GM/WM/CSF fraction as well as T_1 relaxation.

We created 3D maps of concentration estimates for all metabolites and filtered these based on a spectral quality mask, motivated by recent consensus recommendations,⁵⁴ which excluded voxels with at least one of these parameter restrictions: tCr SNR < 5, tCr FWHM > 0.15 ppm, metabolite Cramér-Rao lower bound (CRLB) > 40%, and metabolite fit value > 13 median absolute deviations. For display purposes, these maps were interpolated tri-linearly to fourfold resolution in MINC's register tool.

FreeSurfer (6.0, Laboratory for Computational Neuroimaging at the Athinoula A. Martinos Center for Biomedical Imaging, Boston, MA)^{55,56} was used for automated segmentation of structural images based on cortical and subcortical brain atlases.^{56,57} In-house MATLAB codes were used for mask extraction within each region of interest (ROI). We defined 55 ROIs, as shown in Table 3, including small and large structures/cortices, GM and WM regions separated and merged, and ROIs per hemisphere, in order to investigate which brain regions and ROI sizes could be reliably imaged. Metabolic maps were interpolated to the 0.8 mm resolution of structural images using nearest-neighbor interpolation. Interpolated maps were overlaid with derived masks and mean metabolite concentrations were calculated within each ROI.⁵⁸

2.4 | Data evaluation

2.4.1 | General overview of measurement quality

Metabolite maps of all subjects were controlled by a reader (G.H.) for the presence of lipid and movement artifacts. Quantification of all metabolites listed in the basis set was evaluated and metabolites that were not fit in at least 10% of brain voxels were discarded from further evaluation. Cysteine was discarded as well due to general doubts about its quantification. We compared concentration estimate maps with uncorrected metabolite maps for differences in data quality and contrast. Representative spectra and metabolite maps were selected for display.

2.4.2 | Quantification quality within ROIs

Regions

Region-specific data quality was assessed by calculating the percentage of voxels within an ROI that had CRLBs less than 40% for all of NAA, tCr, tCho, and mIns. ROIs with more than 80% of voxels above that threshold were defined as good and those with 66-79% as acceptable, and those with less than 60% were rejected. Rejected ROIs were excluded from further evaluation. To also quantify the performance of individual metabolite fitting, the percentage of voxels with CRLBs less than 20% for NAA, tCr, tCho, Ins, and CRLBs less than 40% for all others were determined for every ROI.

2.4.3 | Metabolites

Only metabolites that were fit in more than 66% of voxels (mean of all regions) were considered as qualified for the main analysis, but the remaining ones are included in the Supporting Information (Supporting Tables 3 and 4).

2.4.4 | Quantification estimates

For all metabolites in all qualified ROIs, regional means per subject and inter-subject mean of means for all subjects not excluded in Section 2.4.1 were calculated. The range of observed ROI concentration estimates was compared with literature values. To facilitate the comparison with other studies that used ratios to tCr, we additionally calculated metabolite ratios to tCr.

2.4.5 | Inter-subject coefficients of variation

As a measure for the expected variability in metabolite estimates based on physiologic differences among subjects and the stability of our MRSI method, inter-subject coefficients of variation (CVs) of mean ROI-specific concentration estimates and ratios to tCr were calculated and compared

for all qualified ROIs and metabolites based on the mean concentration estimates/ratios per subject for every ROI. This mean and its standard deviation were then used for CV calculation per ROI over all subjects.

3 | RESULTS

3.1 | General overview of measurement quality

One dataset (Volunteer 1) was impaired by strong movement artifacts and had to be excluded from further analysis. In five subjects, some ROIs had to be excluded (Table 1), as the GM/WM classification based on T_1 -weighted imaging had failed in these ROIs. In these ROIs, mean concentration estimates were calculated for the remaining subjects. Total Cr SNR and FWHM over all volunteer brain voxels within the quality mask were 11 ± 5 and 0.06 ± 0.02 ppm. Asp and slns were the only metabolites that were completely excluded from further analysis. Generally, fitting was of good quality, as illustrated by sample spectra in Figure 1 and Supporting Figure 2. Comparison of metabolite maps before T_1 correction and water referencing with concentration estimate maps showed that the concentration estimate maps showed a slight reduction of inhomogeneities and fewer outliers at the brain periphery (Figure 2). The latter was related to the inclusion of GM/WM segmentation, which removed CSF-dominant voxels from the maps. As our extensive 3D metabolite maps cannot satisfactorily be displayed with a limited number of figures, we supplied multiple complete datasets for review (see Section 4.5).

3.2 | Quantification quality within ROIs

3.2.1 | Regions

Of the 55 segmented regions, 18 fulfill the criteria for “good,” 26 for “acceptable,” and 11 were rejected, as detailed in Table 3, including the mean ROI sizes. Concentration estimate standard deviations are generally higher for smaller regions. The rejected regions were mostly situated in

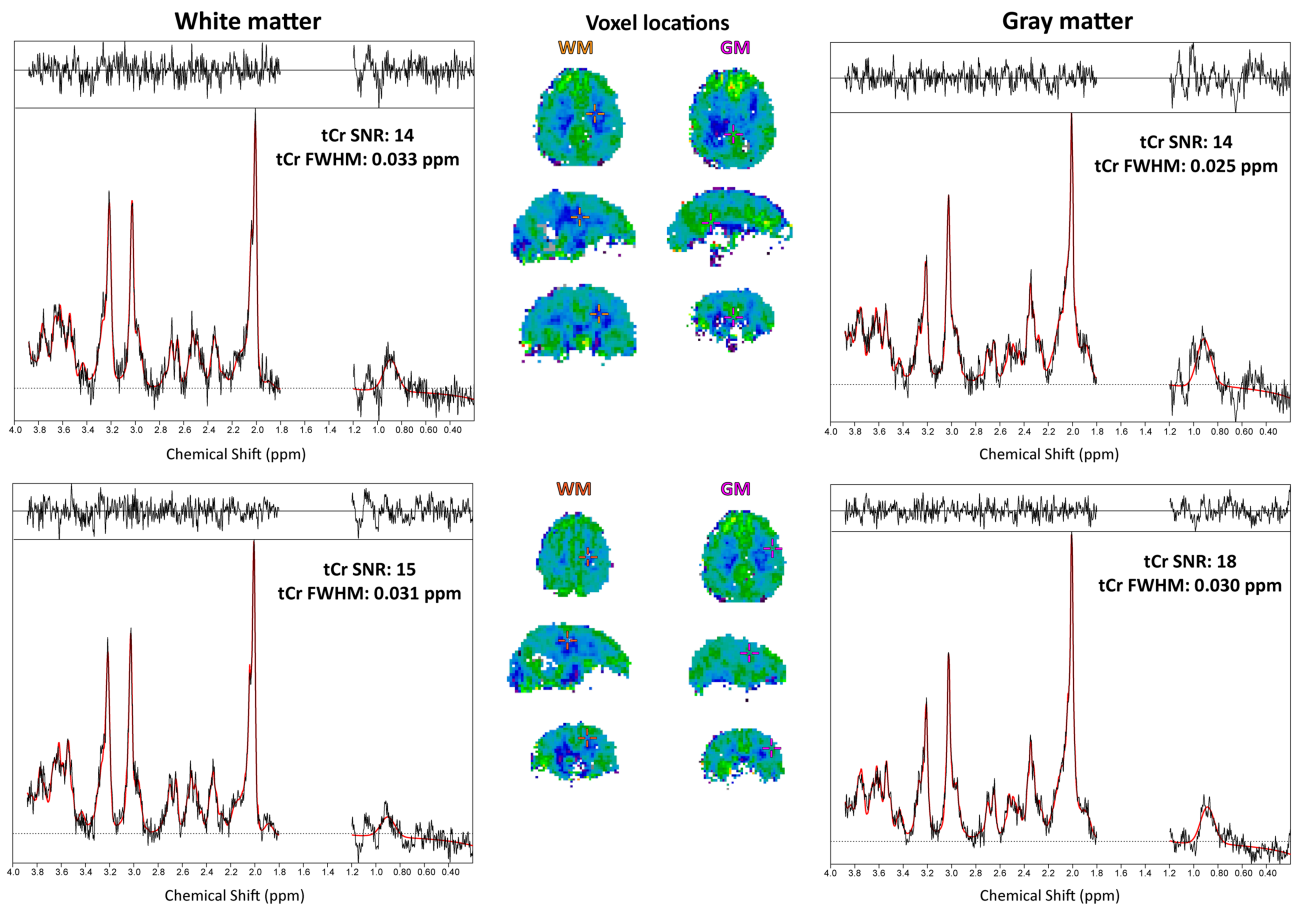


FIGURE 1 Sample spectra for pure GM and WM voxels in Volunteer 11. The spectra were first-order phased for viewing convenience. GM/WM differences are especially visible for Glu. Spectral phasing is due to the 1.3 ms acquisition delay. In these examples, only small residual lipid signals remain visible

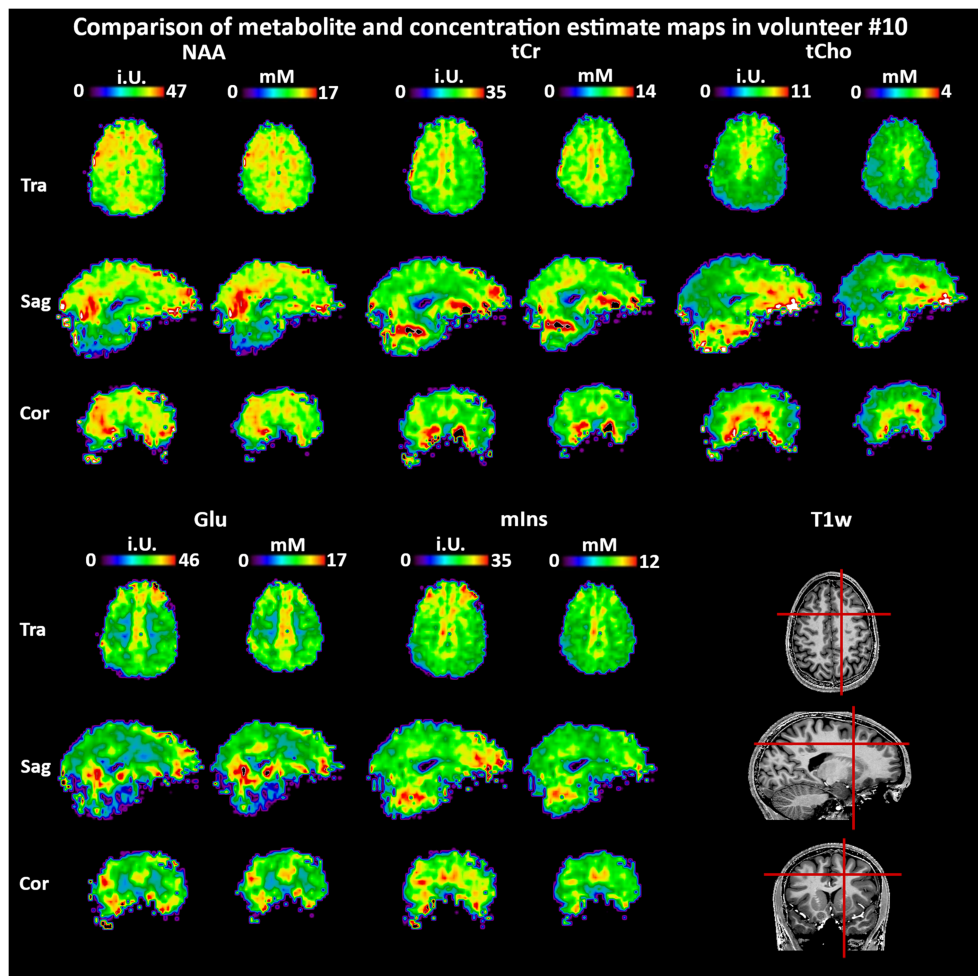


FIGURE 2 Comparison of metabolite maps prior to water referencing and T_1 corrections with concentration estimate maps in one volunteer for the main metabolites. T_1 corrections and water referencing appear to reduce regional variations (eg the transversal tCho maps) while concentration estimates are in general accord with previous literature. Due to the inclusion of segmentation data in the map calculation, more fringe voxels are filtered out, causing the concentration estimate maps to appear smaller

the lower parts of the brain, were small, or were close to the nasal cavities/eyes. Of all metabolites, tCho, tCr, Glu, mIns, and NAA fulfilled the qualification criterion of being fit in more than 66% of voxels (Table 3). An overview over tCr SNR, FWHM, and metabolite CRLBs in relation to the resulting concentration estimate maps is given in Supporting Figure 3.

3.2.2 | Metabolites

Of all cortices, the parietal, motor, and cingulate cortices performed the best.

3.3 | Quantification estimates

Our concentration estimates for the five qualified metabolites over 44 ROIs are presented in Table 4 and graphically summarized in Figure 4. The highest apparent concentrations were found for tCr, Glu, and NAA. Over all ROIs, the minimum and maximum obtained means [mM] were 1.37-2.42 for tCho, 5.93-9.36 for tCr, 6.18-10.14 for Glu, 4.31-6.60 for mIns, and 7.12-10.86 for NAA. We found a high variability between different ROIs. Our estimates were generally within the range of published research for all metabolites. A comparison of our results with previously published concentration estimates^{35,37,59} is shown in Table 5. Metabolite ratios to tCr per ROI are summarized in Supporting Table 1.

TABLE 4 Mean concentration estimates per ROI [mM] and their standard deviations for all qualified metabolites in all qualified ROIs

ROI	tCho	tCr	Glu	mIns	NAA
Subcortical WM (left)	1.89 ± 0.76	7.24 ± 2.72	7.68 ± 3.35	5.15 ± 1.92	9.78 ± 3.77
Subcortical WM (right)	1.95 ± 0.71	7.25 ± 2.50	7.67 ± 3.23	5.35 ± 1.77	9.67 ± 3.44
Subcortical WM (bilateral)	1.92 ± 0.73	7.24 ± 2.62	7.67 ± 3.29	5.24 ± 1.85	9.73 ± 3.61
Motor subcortex WM	2.00 ± 0.47	7.96 ± 1.61	7.90 ± 2.25	5.45 ± 1.15	10.72 ± 2.11
Motor cortex GM	1.71 ± 0.50	7.55 ± 2.06	8.42 ± 2.58	5.39 ± 1.72	10.15 ± 2.79
Motor cortex/subcortex GM+WM	1.87 ± 0.50	7.78 ± 1.83	8.13 ± 2.41	5.42 ± 1.43	10.48 ± 2.44
Parietal subcortex WM	1.84 ± 0.51	7.51 ± 2.00	7.64 ± 2.61	5.54 ± 1.38	10.21 ± 2.66
Parietal cortex GM	1.64 ± 0.50	7.57 ± 2.23	8.55 ± 2.81	5.61 ± 1.63	10.09 ± 3.02
Parietal cortex/subcortex GM+WM	1.74 ± 0.52	7.54 ± 2.11	8.07 ± 2.74	5.58 ± 1.50	10.15 ± 2.83
Cingulate subcortex WM	2.32 ± 0.81	7.55 ± 2.75	8.06 ± 3.70	5.99 ± 2.01	10.55 ± 3.57
Cingulate cortex GM	2.22 ± 0.74	8.45 ± 2.62	10.14 ± 3.57	6.60 ± 2.05	10.86 ± 3.41
Cingulate cortex/subcortex GM+WM	2.28 ± 0.78	7.94 ± 2.73	8.98 ± 3.79	6.26 ± 2.05	10.68 ± 3.51
Visual subcortex WM	1.54 ± 0.57	6.74 ± 2.44	6.64 ± 3.18	4.60 ± 1.62	9.31 ± 3.69
Primary somatosensory subcortex WM	1.73 ± 0.50	7.57 ± 1.93	7.88 ± 2.27	5.21 ± 1.27	10.06 ± 2.57
Primary somatosensory cortex/subcortex GM+WM	1.65 ± 0.52	7.40 ± 2.14	7.90 ± 2.48	5.16 ± 1.46	9.73 ± 2.84
Thalamus	2.40 ± 0.83	8.81 ± 3.07	9.18 ± 4.15	6.24 ± 2.21	10.60 ± 4.00
Putamen	2.27 ± 0.86	9.36 ± 3.32	9.20 ± 3.59	5.09 ± 2.04	9.58 ± 3.77
Non-lobe WM	2.42 ± 0.76	7.59 ± 2.53	6.18 ± 2.75	5.34 ± 1.71	9.88 ± 3.14
Cortical GM (left)	1.64 ± 0.76	6.92 ± 3.06	8.13 ± 3.99	5.06 ± 2.28	9.16 ± 4.47
Cortical GM (right)	1.75 ± 0.64	7.25 ± 2.58	8.35 ± 3.35	5.49 ± 1.91	9.52 ± 3.49
Cortical GM (bilateral)	1.69 ± 0.71	7.07 ± 2.85	8.23 ± 3.70	5.26 ± 2.12	9.33 ± 4.05
Cortical GM+ subcortical WM (left)	1.78 ± 0.77	7.09 ± 2.89	7.89 ± 3.67	5.11 ± 2.10	9.49 ± 4.14
Cortical GM+ subcortical WM (right)	1.86 ± 0.69	7.25 ± 2.54	7.98 ± 3.31	5.41 ± 1.84	9.60 ± 3.47
Cortical GM+ subcortical WM (bilateral)	1.81 ± 0.73	7.16 ± 2.73	7.93 ± 3.50	5.25 ± 1.98	9.54 ± 3.83
Subcortical GM (left)	2.32 ± 0.95	8.61 ± 3.64	8.20 ± 4.06	5.58 ± 2.48	9.50 ± 4.21
Subcortical GM (right)	2.02 ± 0.97	7.40 ± 3.68	7.24 ± 4.16	4.99 ± 2.48	7.83 ± 4.32
Subcortical GM (bilateral)	2.17 ± 0.97	7.99 ± 3.72	7.72 ± 4.15	5.28 ± 2.51	8.66 ± 4.35
Auditory subcortex WM	1.91 ± 0.72	7.13 ± 2.48	8.14 ± 3.23	5.13 ± 1.79	8.81 ± 3.45
Auditory cortex GM	1.67 ± 0.69	6.69 ± 2.60	8.10 ± 3.43	4.88 ± 1.95	8.13 ± 3.56
Auditory cortex/subcortex GM+WM	1.78 ± 0.71	6.89 ± 2.56	8.11 ± 3.34	4.99 ± 1.88	8.44 ± 3.53
Occipital subcortex WM	1.61 ± 0.68	6.61 ± 2.66	6.68 ± 3.35	4.59 ± 1.79	8.83 ± 3.91
Occipital cortex GM	1.46 ± 0.65	6.55 ± 2.92	7.26 ± 3.72	4.57 ± 2.00	8.58 ± 4.31
Occipital cortex/subcortex GM+WM	1.54 ± 0.67	6.58 ± 2.79	6.95 ± 3.55	4.58 ± 1.89	8.71 ± 4.12
Temporal subcortex WM	1.95 ± 0.89	6.89 ± 3.17	7.30 ± 3.68	4.83 ± 2.15	8.56 ± 4.06
Temporal cortex/subcortex GM+WM	1.84 ± 0.87	6.74 ± 3.19	7.47 ± 3.91	4.82 ± 2.21	8.33 ± 4.63
Frontal subcortex WM	1.99 ± 0.79	7.39 ± 2.69	7.99 ± 3.41	5.20 ± 1.92	9.91 ± 3.81
Frontal cortex GM	1.74 ± 0.79	6.98 ± 3.01	8.29 ± 3.98	5.22 ± 2.29	9.44 ± 3.98
Frontal cortex/subcortex GM+WM	1.88 ± 0.80	7.21 ± 2.84	8.12 ± 3.67	5.21 ± 2.09	9.70 ± 3.89
Visual cortex GM	1.37 ± 0.55	6.74 ± 2.72	7.28 ± 3.46	4.53 ± 1.81	9.17 ± 3.99
Visual cortex/subcortex GM+WM	1.46 ± 0.57	6.73 ± 2.57	6.90 ± 3.32	4.56 ± 1.71	9.23 ± 3.83
Primary somatosensory cortex GM	1.57 ± 0.53	7.22 ± 2.33	7.91 ± 2.69	5.11 ± 1.63	9.37 ± 3.06
Pallidum	2.11 ± 0.94	8.88 ± 3.75	8.18 ± 4.30	4.31 ± 2.03	8.43 ± 4.06
Hippocampus	2.18 ± 1.01	7.37 ± 3.35	6.83 ± 3.67	5.78 ± 2.74	7.12 ± 3.73
Corpus callosum	2.07 ± 0.88	5.93 ± 2.62	6.54 ± 3.46	5.25 ± 2.31	9.50 ± 4.28
Mean	1.88	7.37	7.85	5.23	9.43
Min	1.37	5.93	6.18	4.31	7.12
Max	2.42	9.36	10.14	6.60	10.86

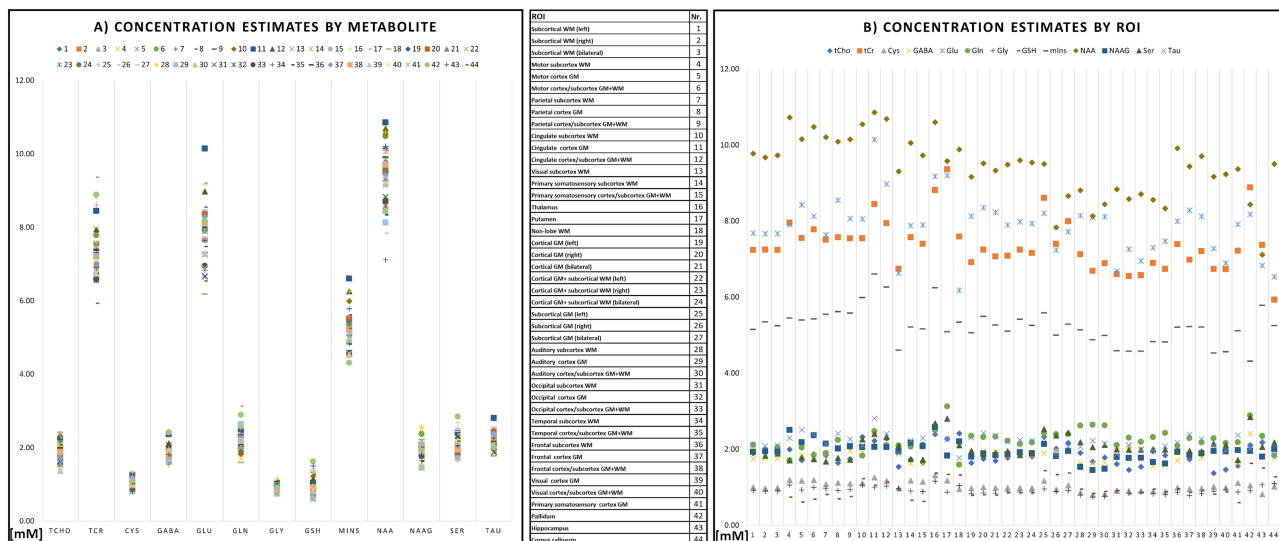


FIGURE 4 Scatterplots of the metabolite concentration estimates presented in Table 4 and Supporting Table 3. A, Estimated concentrations per metabolite; B, estimated concentrations per ROI

TABLE 5 Overview of concentration estimation results of this study compared with those in the literature. A breakdown of reference concentration estimate and literature source ROIs is given in Section 4. An analysis per ROI is presented in Table 7

Metabolite	This study: lowest [mM]	Literature: lowest [mM]	This study: highest [mM]	Literature: highest [mM]	Agreement	References
tCho	1.4	0.5	2.4	4	High	Kreis 1993, Hetherington 1994, Pouwels 1998, Gasparovic 2006, Minati 2010, van de Bank 2015, Lecocq 2015, Volk 2018
tCr	5.9	1.8	9.4	14	High	Kreis 1993, Hetherington 1994, Pouwels 1998, Gasparovic 2006, Minati 2010, van de Bank 2015, Lecocq 2015, Volk 2018, Dhamala 2019
GABA	1.6	1.3	2.5	3.5	High	van Zijl 1997, van de Bank 2015, Dhamala 2019, Gonen 2020
Glu	6.2	5	10.1	12	High	Pouwels 1998, Choi 2006, van de Bank 2015, Volk 2018, Dhamala 2019, Gonen 2020
Gln	1.6	1	3.1	5	High	Pouwels 1998, Choi 2006, van de Bank 2015, Dhamala 2019
Gly	0.8	1	1.2	1	High	van Zijl 1997
GSH	0.6	0.7	1.6	2.2	Moderate	Terpstra 2005, Emir 2011, van de Bank 2015, Rai 2018, Dhamala 2019, Gonen 2020
mlns	4.3	3	6.6	9	High	Kreis 1993, Pouwels 1998, Minati 2010, van de Bank 2015, Lecocq 2015, Volk 2018, Dhamala 2019
NAA	7.1	5	10.9	17	High	Kreis 1993, Hetherington 1994, Pouwels 1998, Gasparovic 2006, Minati 2010, van de Bank 2015, Lecocq 2015, Volk 2018, Dhamala 2019
NAAG	1.5	0.5	2.6	3	High	Pouwels 1997, Pouwels 1998, Edden 2007, Dhamala 2019
Ser	1.7	—	2.9	—	—	—
Tau	1.8	1.5	2.8	2.3	Moderate	van Zijl 1997, van de Bank 2015

3.4 | Inter-subject coefficients of variation

The inter-subject CVs in Table 6 show a good comparability of the regional analyses between subjects for most cases. These CVs were the lowest for tCr and NAA and, generally, in the range of 10-20%. In the majority of “good” ROIs, tCho, tCr, Glu, mlns, and NAA CVs were 10% or less.

TABLE 6 Inter-subject CVs of the concentration estimates per ROI displayed in Table 4. As expected, higher SNR/concentration metabolites corresponded to the lowest CVs

ROI	tCho [%]	tCr [%]	Glu [%]	mIns [%]	NAA [%]
Subcortical WM (left)	7	7	7	8	7
Subcortical WM (right)	6	6	8	6	6
Subcortical WM (bilateral)	6	6	7	7	6
Motor subcortex WM	8	7	7	7	7
Motor cortex GM	6	8	8	8	9
Motor cortex/subcortex GM + WM	7	7	7	8	8
Parietal subcortex WM	11	10	10	10	10
Parietal cortex GM	10	10	11	10	11
Parietal cortex/subcortex GM + WM	10	10	11	10	11
Cingulate subcortex WM	9	10	12	10	9
Cingulate cortex GM	9	10	12	10	10
Cingulate cortex/subcortex GM + WM	9	10	12	10	9
Visual subcortex WM	13	15	14	14	8
Primary somatosensory subcortex WM	8	9	8	10	8
Primary somatosensory cortex/subcortex GM + WM	8	9	8	10	9
Thalamus	19	20	21	19	16
Putamen	9	9	15	13	11
Non-lobe WM	10	7	15	10	8
Cortical GM (left)	7	8	7	8	8
Cortical GM (right)	6	6	7	6	6
Cortical GM (bilateral)	6	6	7	7	7
Cortical GM + subcortical WM (left)	7	7	7	8	8
Cortical GM + subcortical WM (right)	6	6	7	6	6
Cortical GM + subcortical WM (bilateral)	6	6	7	7	6
Subcortical GM (left)	10	9	14	13	10
Subcortical GM (right)	15	15	16	14	15
Subcortical GM (bilateral)	12	11	15	13	11
Auditory subcortex WM	8	9	9	10	9
Auditory cortex GM	7	8	8	8	9
Auditory cortex/subcortex GM + WM	7	8	9	9	9
Occipital subcortex WM	12	12	12	12	7
Occipital cortex GM	11	12	10	12	7
Occipital cortex/subcortex GM + WM	11	12	11	12	6
Temporal subcortex WM	6	8	7	9	8
Temporal cortex/subcortex GM + WM	5	8	7	8	8
Frontal subcortex WM	8	7	10	9	8
Frontal cortex GM	8	7	9	8	9
Frontal cortex/subcortex GM + WM	8	7	9	9	8
Visual cortex GM	13	17	12	15	8
Visual cortex/subcortex GM + WM	13	16	12	14	7
Primary somatosensory cortex GM	8	10	9	10	9
Pallidum	14	12	24	15	19
Hippocampus	16	17	18	18	16
Corpus callosum	16	16	19	15	17

TABLE 6 (Continued)

ROI	tCho [%]	tCr [%]	Glu [%]	mIns [%]	NAA [%]
Mean	9	10	11	10	9
Min.	5	6	7	6	6
Max.	19	20	24	19	19

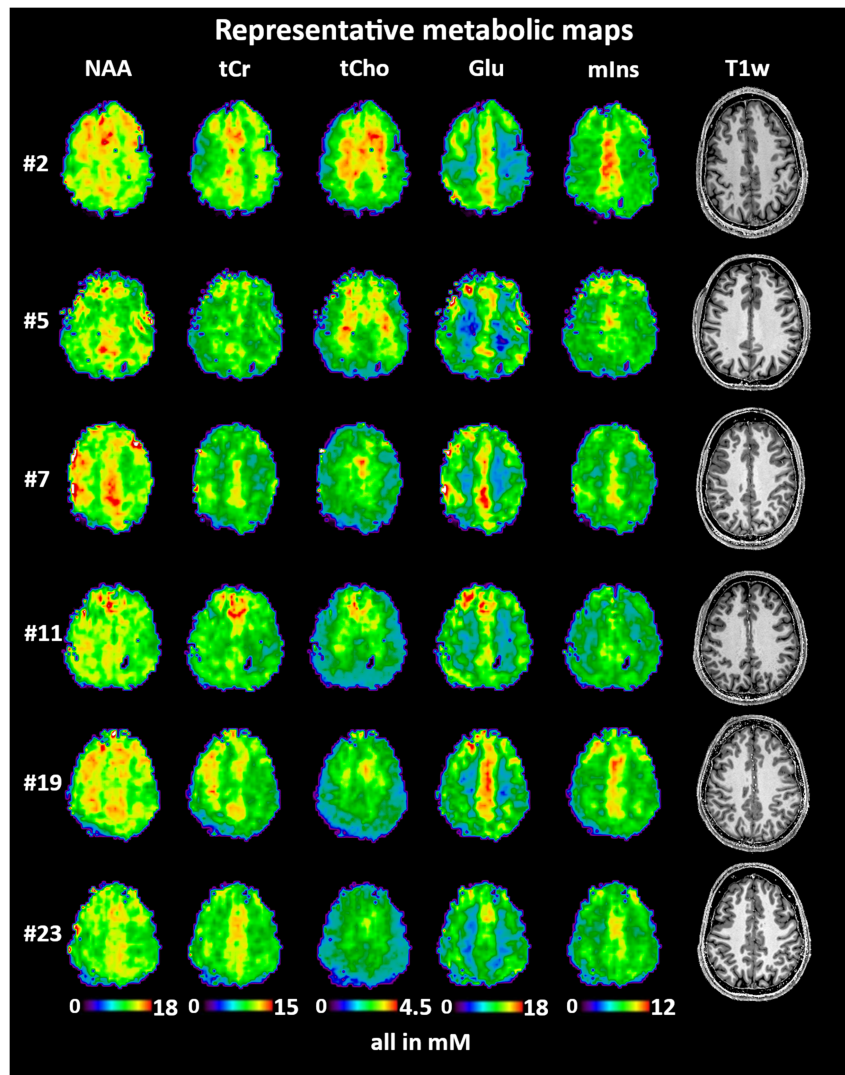


FIGURE 3 Visualization of data consistency of concentration estimates in six volunteer subjects for NAA, tCr, tCho, Glu, and mIns. Presented is a transversal MRSI slice location directly above the ventricles in all subjects. Full map datasets for a detailed inspection of all metabolite concentration estimate maps of Volunteers 7, 11, 13, 19, and 23 are available at Zenodo (<https://doi.org/10.5281/zenodo.5006923>)

Figure 3 illustrates these findings over multiple subjects. The CVs for ratios to tCr (Supporting Table 2) were very similar, with differences between the means over all ROIs not exceeding 4%.

4 | DISCUSSION

We have assessed the average and region-specific concentration estimates, as well as their inter-subject variability, for five neuro-metabolites that can be reliably mapped in the human brain using our 3D-CRT-based FID-MRSI sequence at 7 T. To improve upon previous work,²¹ we have

expanded the subject cohort, also evaluated less abundant metabolites, and assessed concentration estimates instead of ratios and data quality over a large number of automatically segmented brain ROIs to provide a more detailed understanding of the performance of 7 T 3D-CRT-based FID-MRSI. The additional inclusion of T_1 corrections and internal water referencing allowed a more quantitative assessment (ie of concentration estimates). In summary, we found our method to yield acceptable results in 23 of 24 volunteer subjects for five metabolites in 44 predefined ROIs. Our concentration estimates are in the range of previous reports, while inter-subject CVs indicated a good level of stability in many of these metabolites and ROIs. Still, the quantification quality of GABA, Gln, Gly, GSH, NAAG, Ser, and Tau in healthy subjects cannot be considered sufficient for this MRSI application, necessitating different approaches or methodological improvements if these are required. These results are important to define the limits of stability, sensitivity, and regional reliability for our MRSI method for future research applications. As the sum of our

TABLE 7 Comparison of this study's concentration estimates and their standard deviations in specific ROIs to literature. The details of this comparison are elaborated on in Section 4

Source	tCho	tCr	Glu	mIns	NAA
<i>Occipital GM</i>					
This study	1.46 ± 0.65	6.55 ± 2.92	7.26 ± 3.72	4.57 ± 2.00	8.58 ± 4.31
Kreis 1993	1.41 ± 0.05	7.95 ± 0.11	–	6.24 ± 0.21	9.06 ± 0.12
Pouwels 1998	0.88 ± 0.10	6.90 ± 0.70	8.60 ± 1.10	4.10 ± 0.60	9.20 ± 0.90
Lecocq 2015	1.20-1.40	7.30 8.70	–	3.50-4.60	9.50-12.10
<i>Occipital WM</i>					
This study	1.61 ± 0.68	6.61 ± 2.66	6.68 ± 3.35	4.59 ± 1.79	8.83 ± 3.91
Pouwels 1998	1.64 ± 0.21	5.50 0.80	6.00 ± 1.20	4.10 ± 0.80	7.80 ± 0.90
Lecocq 2015	1.20-1.40	7.30 8.70	–	3.50-4.60	9.50-12.10
<i>Frontal GM</i>					
This study	1.74 ± 0.79	6.98 ± 3.01	8.29 ± 3.98	5.22 ± 2.29	9.44 ± 3.98
Pouwels 1998	1.38 ± 0.17	6.40 ± 0.70	8.50 ± 1.00	4.30 ± 0.90	7.70 ± 1.00
Lecocq 2015	1.50 ± 2.50	6.70 ± 8.60	–	4.00 ± 7.80	9.50 ± 12.50
<i>Frontal WM</i>					
This study	1.99 ± 0.79	7.39 ± 2.69	7.99 ± 3.41	5.20 ± 1.92	9.91 ± 3.81
Pouwels 1998	1.78 ± 0.41	5.70 ± 0.50	7.00 ± 2.60	3.80 ± 0.90	8.10 ± 0.90
Minati 2010	3.60 ± 0.80	11.50 ± 2.40	–	7.60 ± 2.00	14.20 ± 2.00
Lecocq 2015	1.50 ± 2.50	6.70 ± 8.60	–	4.00 ± 7.80	9.50 ± 12.50
<i>Parietal lobe</i>					
This study	1.74 ± 0.52	7.54 ± 2.11	8.07 ± 2.74	5.58 ± 1.50	10.15 ± 2.83
Lecocq 2015	0.80-1.10	4.10-6.50	–	1.90-3.20	8.30-10.70
Volk 2018	1.65 ± 0.05	7.54 ± 0.14	12.55 ± 0.22	3.70 ± 0.08	11.59 ± 0.13
<i>Thalamus</i>					
This study	2.40 ± 0.83	8.81 ± 3.07	9.18 ± 4.15	6.24 ± 2.21	10.60 ± 4.00
Minati 2010	3.40 ± 0.80	12.00 ± 1.10	–	6.60 ± 1.80	16.30 ± 2.00
Lecocq 2015	1.20-1.30	5.90-6.60	–	3.00-3.30	5.90-6.60
<i>Temporal cortex</i>					
This study	1.84 ± 0.87	6.74 ± 3.19	7.47 ± 3.91	4.82 ± 2.21	8.33 ± 4.63
Minati 2010	3.60 ± 1.10	12.00 ± 4.00	–	7.90 ± 3.00	14.10 ± 2.50
Lecocq 2015	1.40-2.30	7.50-8.80	–	4.20-5.30	8.80-10.90
<i>Cingulate subcortex</i>					
This study	2.28 ± 0.78	7.94 ± 2.73	8.98 ± 3.79	6.26 ± 2.05	10.68 ± 3.51
Hetherington 1994	2.30 ± 0.40	7.70 ± 0.90	–	–	13.50 ± 0.90
van de Bank 2015	1.30 ± 0.10	8.10 ± 0.50	9.40 ± 0.80	6.40 ± 0.60	12.10 ± 1.00
Lecocq 2015	1.00-2.50	5.90-9.30	–	3.20-6.40	7.90-11.50
Gonen 2020	–	–	10.20 ± 1.80	–	–

Some publications used more ROIs without GM/WM separation per region and the results are therefore presented as a range of their findings.

generated imaging data is hard to convey within few figures, we invite the readers to look at the supplementary full datasets provided by us on Zenodo.

To contextualize our resultant metabolite distributions, we conducted an extensive comparison with previous research. Concentration estimates for many metabolites in many brain regions have been reported over the last decades, sometimes with contradicting results due to different processing methods, subject cohorts, partial volume effects, acquisition schemes (eg MRSI or single-voxel spectroscopy, SVS), and scanner types. Different quantification algorithms are known to affect reported results.⁶⁰ Dhamala et al³⁷ found that correlations varied strongly for different metabolites between different MRS methods in the same subjects. A comparison with our 7 T-FID-MRSI method with 3.4 mm nominal isometric resolution, a T_R of 450 ms, and an acquisition delay of 1.3 ms remains challenging. Nonetheless, our results are, overall, consistent with previously reported concentration estimates^{31–37,53,61–69} as summarized in Table 5, and mostly found in the middle or lower range of references. For metabolites separable in our study, such as Glu/Gln and NAA/NAAG, they individually agree with previous literature (Tables 5 and 7), and further comparing their sums agrees well with studies that cannot separate them.

Going from overall reported values to specific ROIs, as compared in Table 7, we found similar concentrations (within the respective standard deviations of each other) in occipital GM and WM,^{31,32,35} frontal WM,^{32,35} parietal lobe,³⁶ thalamus,³⁴ temporal cortex,³⁵ and cingulate cortex^{33,63} for most studies. We found disagreements beyond a standard deviation for the cingulate cortex with van de Bank et al,⁶⁸ for the frontal WM, thalamus, and temporal cortex with Minati et al,³⁴ and for the parietal cortex as well as the thalamus with Lecocq et al.³⁵

For metabolite ratios to tCr, we also compared our results with the 7 T MRSI results of Bhogal et al,⁷⁰ as seen in Table 8. Over the six compared ROIs, our ratios are consistently higher for all except GSH/tCr, which is mixed. The effect is most pronounced for Ins + Gly. The generally higher ratios could be sourced in lower quantification estimates of tCr or differences in the MRSI acquisition.

For some metabolites, previous concentration estimates are only reported sparsely. Our 0.76–1.16 mM of Gly align well to the 1.02 mM in Reference⁶⁴ and to a Gly/tCr of 0.14 in Reference,⁷¹ which compares well with our range of 0.08–0.17 for Gly/tCr. We established concentrations of 1.68–2.85 mM for Ser, with a ratio to tCr of 0.8 in Reference,⁷² which that was published in the MRS literature. Our Ser/tCr of 0.21–0.36 is notably lower. For Tau, we found 1.77–2.81 mM, which is higher than the 1.48 mM reported in Reference,⁶⁴ but well aligned with the 2.3 mM for Tau + glucose in Reference.⁶⁸

Considering the multitude of applied methods and overall limited sample sizes, our results are in general agreement with the current state of knowledge in the field but are for the first time based on concentration estimation for high-resolution 7 T FID-MRSI. We see a further need to investigate metabolites such as GSH, Ser, and Tau, which are difficult to quantify and for which MRS-based concentration estimates are scarce.

Our inter-subject CVs were the smallest for metabolites with the highest SNR (ie, NAA, tCr, tCho, Glu, and mIns are in the <10% range) but approached 30% for other metabolites in some ROIs (see Table 6). Comparison with the literature is difficult, as most studies report intra-subject

TABLE 8 Comparison of this study's metabolite ratios and standard deviations of tCho, Glu, Glu + Gln, NAA + NAAG, Ins + Gly, and GSH to tCr in six ROIs compared with similar 7 T MRSI results of Reference.⁷⁰ The results of our study are consistently higher for all except GSH/tCr, with two higher/lower/same ratio regions each

Source	tCho/tCr	Glu/tCr	(Glu + Gln)/tCr	(NAA + NAAG)/tCr	(Ins + Gly)/tCr	GSH/tCr
<i>(Cortical) GM</i>						
This study	0.24 ± 0.01	1.17 ± 0.09	1.50 ± 0.10	1.59 ± 0.09	0.86 ± 0.04	0.11 ± 0.01
Bhogal 2020	0.17 ± 0.05	0.97 ± 0.20	1.20 ± 0.27	1.13 ± 0.28	0.41 ± 0.16	0.15 ± 0.06
<i>(Subcortical) WM</i>						
This study	0.27 ± 0.02	1.07 ± 0.09	1.34 ± 0.10	1.62 ± 0.09	0.85 ± 0.04	0.12 ± 0.01
Bhogal 2020	0.22 ± 0.04	0.72 ± 0.14	0.88 ± 0.17	1.27 ± 0.20	0.41 ± 0.11	0.15 ± 0.04
<i>Corpus callosum</i>						
This study	0.35 ± 0.03	1.13 ± 0.28	1.38 ± 0.10	1.97 ± 0.27	1.06 ± 0.13	0.21 ± 0.04
Bhogal 2020	0.23 ± 0.04	0.73 ± 0.13	0.90 ± 0.16	1.26 ± 0.22	0.45 ± 0.09	0.17 ± 0.04
<i>Pallidum</i>						
This study	0.24 ± 0.02	0.90 ± 0.17	1.20 ± 0.20	1.15 ± 0.15	0.56 ± 0.07	0.17 ± 0.03
Bhogal 2020	0.18 ± 0.01	0.58 ± 0.10	0.71 ± 0.12	0.85 ± 0.19	0.31 ± 0.06	0.15 ± 0.04
<i>Thalamus</i>						
This study	0.28 ± 0.03	1.07 ± 0.24	1.34 ± 0.26	1.53 ± 0.16	0.83 ± 0.14	0.15 ± 0.04
Bhogal 2020	0.22 ± 0.03	0.75 ± 0.10	0.93 ± 0.12	1.07 ± 0.12	0.36 ± 0.09	0.15 ± 0.02
<i>Putamen</i>						
This study	0.24 ± 0.01	0.98 ± 0.12	1.30 ± 0.14	1.23 ± 0.08	0.63 ± 0.05	0.14 ± 0.03
Bhogal 2020	0.19 ± 0.02	0.78 ± 0.10	0.97 ± 0.13	0.84 ± 0.14	0.32 ± 0.06	0.15 ± 0.03

or inter-system CVs, such as van de Bank et al,⁶⁸ who reported CVs for SVS on four different 7 T systems in the posterior cingulate cortex of 3-4% for NAA, tCho, tCr, mIns, and Glu, 22.2% for GABA, 14.4% for GSH, and 8.8% for Gln. Another example, but at 3 T, is the study by Zhang et al,⁷³ who calculated intra-subject CVs for whole-brain EPSI in 10 volunteers over three scans in 47 ROIs and found NAA CVs of 3.3%-17.8%, tCho CVs of 3.7%-31.0%, tCr CVs of 3.1%-18.0% (with mean ROI CVs < 10%), and mIns CVs of 5.9%-54.0%. Inter-subject CVs for metabolic ratios at 3 T were reported by Veenith et al,⁷⁴ with mean CVs of 21.24% for tCho/tCr and 13.30% for tNAA/tCr. Except for higher mIns CVs, these results are similar to our findings, but our 7 T MRSI featured a higher resolution and more quantifiable metabolites and was also affected by additional physiologic inter-subject variation. Considering that the CV calculation did not account for diurnal effects,³⁶ or age⁷⁵⁻⁷⁷ and sex differences,^{78,79} these results seem convincing but still include methodological artifacts such as subject motion. Intra-subject CVs from a test-retest study will be necessary to complete the picture. In another MRSI study at 3 T, we found that the application of motion correction improved the CVs of metabolite ratios to tCr by 30%.³⁰ Another source of local variability would be the combination of T_1 weighting with our short T_R and a lack of knowledge of local tissue metabolite T_1 values.^{52,80} Although we tried to correct our T_1 estimates and reference water concentrations for voxel-wise GM/WM fractions, we assume that additional variation exists based on this.⁵³ More precise concentration estimates could be obtained via the direct mapping of tissue water content.⁸¹ Due to our echo-less acquisition approach with negligible acquisition delay, our results can be considered to be robust to T_2 effects. This is a potential advantage in the study of the aging brain or of pathologies that can cause local iron deposits, which affect metabolite and water T_2 values.⁸²

4.1 | Limitations

Our study has some limitations. T_1 values for multiple metabolites had to be estimated without previous reports. The assumption of a single metabolite T_1 over the whole brain is also a rough approximation. This could have biased the estimated concentrations.

Quantification is further limited by the precision of the internal water referencing, which relies on the assumption of tissue water relaxation times and concentrations, effective local excitation, and water signal quantification. Beyond the general variability of MRS quantification results based on the fit model parameters, L2 regularization is also known to influence metabolite signal estimation, especially NAA,⁸³ even if just by removing lipid signals. The comparison of quantification estimates between different field strengths, acquisition schemes, processing pipelines, resolutions, and brain segmentations limits the comparability to the even subset of MRS studies that report concentration estimates.

Our study is limited to the analysis of inter-subject variations and does not, therefore, report on intra-subject variations. Measuring intra-subject variation could also help to separate the more subject-specific (eg physiological) from the method-specific contributions to variability.

The exclusion of 11 ROIs, predominantly basal brain regions such as brain stem or cerebellum, from further analysis was necessary due to the lack of spectral fit confidence, limiting the mappable brain coverage. This shows that B_0 - and B_1 -field inhomogeneities (the first caused by the proximity to the nasal and auditory cavities, the second by the limitations of single channel transmit coils at 7 T) remain a significant ultra-high-field challenge, which will have to be resolved via hardware improvements⁸⁴⁻⁸⁶ and/or further improved high-resolution approaches.⁸⁷

Filtering of outliers based on a set of rigid criteria is insufficient. In the future, automated quality assessment of voxels based on deep learning will be necessary to evaluate datasets of this scale adequately. The necessary interpolation between MRSI and reference imaging combined with MRSI partial volume effects, even at our high resolution, are further confounding factors for the regional analysis as relevant GM/WM fractions remain within the ROIs (Table 3), reducing the expected GM/WM contrast, eg for Glu. While we obtained results for difficult-to-quantify metabolites in healthy tissue (ie GABA, Gln, Gly, GSH, NAAG, Ser, and Tau), the percentage of voxels within the quality criteria remained overall low (Table 1).

Subject motion is another factor not yet accounted for in our study, and significant improvements are expected in stability,^{88,89} which is of particular importance for studies in children and elderly patients.²⁶ In particular, real-time correction has been shown to significantly enhance data quality in high-resolution 3D-CRT-based FID-MRSI at 3 T.³⁰

4.2 | Conclusions/outlook

We have established the brain region-specific concentration estimates and their variability in a large number of healthy young volunteers for our whole-brain MRSI-based metabolic maps at 7 T for the first time. While not all brain ROIs performed well enough to be considered, especially basal regions such as the cerebellum, we could successfully quantify five metabolites—tCho, tCr, NAA, Glu, and Ins—in 44 ROIs, with all others not being quantified with a sufficient quality in a substantial number of voxels. Our estimated concentrations are consistent with previous research.

This was a necessary first step to define the reliability and to guide future basic and clinical research of the brain metabolism and to show the capability of our high-resolution 3D-MRSI technique in the current discussion of MRSI standardization.^{52,90,91} Our results can guide future study planning, targeting specific brain regions and metabolites of interest on the one hand and the eventual development of a 7 T-MRSI based metabolic brain atlas on the other. The next avenues of research could be the investigation of intra-subject variability, improved quantification by direct water

concentration mapping,⁸¹ also in pathologies, and better definition of specific relaxation times. With these improvements, the metabolites that currently lack reliability could be reevaluated and an in-depth study of sex and age differences could be carried out. In summary, we have shown new insights into the expectable results and stability of our fast high-resolution MRSI at 7 T, but this approach still requires more sophistication.

ACKNOWLEDGEMENTS

This work was supported by the Austrian Science Fund (FWF) grants KLI-646, P 30701 and P 34198.

CONFLICT OF INTEREST

We have no conflicts of interest to report.

SUPPLEMENTARY MATERIALS/DATA AVAILABILITY STATEMENT

Individual subject concentration estimate map datasets in MINC and NIFTI format including SNR, FWHM, and CRLB maps are available on Zenodo: <https://doi.org/10.5281/zenodo.5006923>.⁹² A summary of the MRSI method used according to the MRSinMRS experts' consensus⁹³ can be found in Supporting Table 5.

DATA AVAILABILITY STATEMENT

Individual subject ROI quantification tables, as well as metabolite and concentration estimate map datasets in MINC and NIFTI format, are available at Zenodo <https://doi.org/10.5281/zenodo.500692392>. A summary of the MRSI method used according to the MRSinMRS expert's consensus can be found in Sup.Tbl. 5.

ORCID

Gilbert Hangel  <https://orcid.org/0000-0002-3986-3159>

Wolfgang Bogner  <https://orcid.org/0000-0002-0130-3463>

REFERENCES

1. Henning A, Fuchs A, Murdoch JB, Boesiger P. Slice-selective FID acquisition, localized by outer volume suppression (FIDLOVS) for ¹H-MRSI of the human brain at 7 T with minimal signal loss. *NMR Biomed*. 2009;22(7):683-696. <https://doi.org/10.1002/nbm.1366>
2. Bogner W, Gruber S, Trattnig S, Chmelik M. High-resolution mapping of human brain metabolites by free induction decay ¹H MRSI at 7T. *NMR Biomed*. 2012;25(6):873-882. <https://doi.org/10.1002/nbm.1805>
3. Moser E, Stahlberg F, Ladd ME, Trattnig S. 7-T MR—from research to clinical applications? *NMR Biomed*. 2012;25(5):695-716. <https://doi.org/10.1002/nbm.1794>
4. Bogner W, Otazo R, Henning A. Accelerated MR spectroscopic imaging—a review of current and emerging techniques. *NMR Biomed*. 2021;34(5):e4314. <https://doi.org/10.1002/nbm.4314>
5. Hangel G, Strasser B, Považan M, et al. Lipid suppression via double inversion recovery with symmetric frequency sweep for robust 2D-GRAPPA-accelerated MRSI of the brain at 7 T. *NMR Biomed*. 2015;28(11):1413-1425. <https://doi.org/10.1002/nbm.3386>
6. Strasser B, Považan M, Hangel G, et al. (2 + 1)D-CAIPIRINHA accelerated MR spectroscopic imaging of the brain at 7T. *Magn Reson Med*. 2017;78(2):429-440. <https://doi.org/10.1002/mrm.26386>
7. Nassirpour S, Chang P, Henning A. MultiNet PyGRAPPA: multiple neural networks for reconstructing variable density GRAPPA (a ¹H FID MRSI study). *NeuroImage*. 2018;183:336-345. <https://doi.org/10.1016/j.neuroimage.2018.08.032>
8. Posse S, Otazo R, Tsai S-Y, Yoshimoto AE, Lin F-H. Single-shot magnetic resonance spectroscopic imaging with partial parallel imaging. *Magn Reson Med*. 2009;61(3):541-547. <https://doi.org/10.1002/mrm.21855>
9. An Z, Tiwari V, Ganji SK, et al. Echo-planar spectroscopic imaging with dual-readout alternated gradients (DRAG-EPSI) at 7 T: application for 2-hydroxyglutarate imaging in glioma patients. *Magn Reson Med*. 2018;79(4):1851-1861. <https://doi.org/10.1002/MRM.26884>
10. Hangel G, Strasser B, Považan M, et al. Ultra-high resolution brain metabolite mapping at 7 T by short-TR Hadamard-encoded FID-MRSI. *NeuroImage*. 2016;168:199-210. <https://doi.org/10.1016/j.neuroimage.2016.10.043>
11. Nassirpour S, Chang P, Henning A. High and ultra-high resolution metabolite mapping of the human brain using 1H FID MRSI at 9.4T. *NeuroImage*. 2016;168:211-221. <https://doi.org/10.1016/j.neuroimage.2016.12.065>
12. Iqbal Z, Nguyen D, Hangel G, Motyka S, Bogner W, Jiang S. Super-resolution ¹H magnetic resonance spectroscopic imaging utilizing deep learning. *Front Oncol*. 2019;9:1010. <https://doi.org/10.3389/fonc.2019.01010>
13. Andronesi OC, Gagoski BA, Sorensen AG. Neurologic 3D MR spectroscopic imaging with low-power adiabatic pulses and fast spiral acquisition. *Radiology*. 2012;262(2):647-661. <https://doi.org/10.1148/radiol.11110277>
14. Esmaeili M, Strasser B, Bogner W, Moser P, Wang Z, Andronesi OC. Whole-slab 3D MR spectroscopic imaging of the human brain with spiral-out-in sampling at 7T. *J Magn Reson Imaging*. 2021;53(4):1237-1250. <https://doi.org/10.1002/jmri.27437>
15. Schirda CV, Zhao T, Andronesi OC, et al. In vivo brain rosette spectroscopic imaging (RSI) with LASER excitation, constant gradient strength readout, and automated LCMoel quantification for all voxels. *Magn Reson Med*. 2016;76(2):380-390. <https://doi.org/10.1002/mrm.25896>
16. Chiew M, Jiang W, Burns B, et al. Density-weighted concentric rings k-space trajectory for 1H magnetic resonance spectroscopic imaging at 7 T. *NMR Biomed*. 2018;31(1):e3838. <https://doi.org/10.1002/nbm.3838>
17. Moser P, Bogner W, Hingerl L, et al. Non-Cartesian GRAPPA and coil combination using interleaved calibration data—application to concentric-ring MRSI of the human brain at 7T. *Magn Reson Med*. 2019;82(5):1587-1603. <https://doi.org/10.1002/mrm.27822>

18. Furuyama JK, Wilson NE, Thomas MA. Spectroscopic imaging using concentric circular echo-planar trajectories in vivo. *Magn Reson Med*. 2012; 67(6):1515-1522. <https://doi.org/10.1002/mrm.23184>
19. Emir UE, Burns B, Chiew M, Jezzard P, Thomas MA. Non-water-suppressed short-echo-time magnetic resonance spectroscopic imaging using a concentric ring k -space trajectory. *NMR Biomed*. 2017;30(7):e3714. <https://doi.org/10.1002/nbm.3714>
20. Hingerl L, Bogner W, Moser P, et al. Density-weighted concentric circle trajectories for high resolution brain magnetic resonance spectroscopic imaging at 7T. *Magn Reson Med*. 2018;79(6):2874-2885. <https://doi.org/10.1002/mrm.26987>
21. Hingerl L, Strasser B, Moser P, et al. Clinical high-resolution 3D-MR spectroscopic imaging of the human brain at 7 T. *Invest Radiol*. 2020;55(4): 239-248. <https://doi.org/10.1097/RLI.0000000000000626>
22. Hangel G, Cadrien C, Lazen P, et al. High-resolution metabolic imaging of high-grade gliomas using 7T-CRT-FID-MRSI. *NeuroImage Clin*. 2020;28: 102433. <https://doi.org/10.1016/j.nicl.2020.102433>
23. Gruber S, Heckova E, Strasser B, et al. Mapping an extended neurochemical profile at 3 and 7 T using accelerated high-resolution proton magnetic resonance spectroscopic imaging. *Invest Radiol*. 2017;52(10):631-639. <https://doi.org/10.1097/RLI.0000000000000379>
24. Hangel G, Jain S, Springer E, et al. High-resolution metabolic mapping of gliomas via patch-based super-resolution magnetic resonance spectroscopic imaging at 7T. *NeuroImage*. 2019;191:587-595. <https://doi.org/10.1016/j.neuroimage.2019.02.023>
25. Moser P, Hingerl L, Strasser B, et al. Whole-slice mapping of GABA and GABA⁺ at 7T via adiabatic MEGA-editing, real-time instability correction, and concentric circle readout. *NeuroImage*. 2019;184:475-489. <https://doi.org/10.1016/j.neuroimage.2018.09.039>
26. Heckova E, Povazan M, Strasser B, et al. Real-time correction of motion and imager instability artifacts during 3D γ -aminobutyric acid-edited MR spectroscopic imaging. *Radiology*. 2018;286(2):666-675. <https://doi.org/10.1148/radiol.2017170744>
27. Ganji SK, An Z, Tiwari V, et al. In vivo detection of 2-hydroxyglutarate in brain tumors by optimized point-resolved spectroscopy (PRESS) at 7T. *Magn Reson Med*. 2017;77(3):936-944. <https://doi.org/10.1002/mrm.26190>
28. Heckova E, Strasser B, Hangel GJ, et al. 7 T magnetic resonance spectroscopic imaging in multiple sclerosis. *Invest Radiol*. 2019;54(4):247-254. <https://doi.org/10.1097/RLI.0000000000000531>
29. Pan JW, Duckrow RB, Gerrard J, et al. 7T MR spectroscopic imaging in the localization of surgical epilepsy. *Epilepsia*. 2013;54(9):1668-1678. <https://doi.org/10.1111/epi.12322>
30. Moser P, Eckstein K, Hingerl L, et al. Intra-session and inter-subject variability of 3D-FID-MRSI using single-echo volumetric EPI navigators at 3T. *Magn Reson Med*. 2020;83(6):1920-1929. <https://doi.org/10.1002/mrm.28076>
31. Kreis R, Ernst T, Ross BD. Absolute quantitation of water and metabolites in the human brain. II. Metabolite concentrations. *J Magn Reson B*. 1993; 102(1):9-19. <https://doi.org/10.1006/jmrb.1993.1056>
32. Pouwels PJW, Frahm J. Regional metabolite concentrations in human brain as determined by quantitative localized proton MRS. *Magn Reson Med*. 1998;39(1):53-60. <https://doi.org/10.1002/mrm.1910390110>
33. Hetherington HP, Mason GF, Pan JW, et al. Evaluation of cerebral gray and white matter metabolite differences by spectroscopic imaging at 4.1T. *Magn Reson Med*. 1994;32(5):565-571. <https://doi.org/10.1002/mrm.1910320504>
34. Minati L, Aquino D, Bruzzone M, Erbetta A. Quantitation of normal metabolite concentrations in six brain regions by in-vivo 1 H-MR spectroscopy. *J Med Phys*. 2010;35(3):154-163. <https://doi.org/10.4103/0971-6203.62128>
35. Lecoq A, Le Fur Y, Maudsley AA, et al. Whole-brain quantitative mapping of metabolites using short echo three-dimensional proton MRSI. *J Magn Reson Imaging*. 2015;42(2):280-289. <https://doi.org/10.1002/jmri.24809>
36. Volk C, Jaramillo V, Merki R, O'Gorman Tuura R, Huber R. Diurnal changes in glutamate + glutamine levels of healthy young adults assessed by proton magnetic resonance spectroscopy. *Hum Brain Mapp*. 2018;39(10):3984-3992. <https://doi.org/10.1002/hbm.24225>
37. Dhamala E, Abdelkefi I, Nguyen M, Hennessy TJ, Nadeau H, Near J. Validation of in vivo MRS measures of metabolite concentrations in the human brain. *NMR Biomed*. 2019;32(3):e4058. <https://doi.org/10.1002/nbm.4058>
38. Ogg RJ, Kingsley PB, Taylor JS. WET, a T_1 - and B_1 -insensitive water-suppression method for *in vivo* localized ^1H NMR spectroscopy. *J Magn Reson B*. 1994;104(1):1-10.
39. Považan M, Strasser B, Hangel G, Gruber S, Trattng S, Bogner W. Multimodal post-processing software for MRSI data evaluation. *Proc Int Soc Magn Reson Med.s* 2015;23:1973.
40. Jackson JI, Meyer CH, Nishimura DG, Macovski A. Selection of a convolution function for Fourier inversion using gridding (computerised tomography application). *IEEE Trans Med Imaging*. 1991;10(3):473-478. <https://doi.org/10.1109/42.97598>
41. Mayer D, Levin YS, Hurd RE, Glover GH, Spielman DM. Fast metabolic imaging of systems with sparse spectra: application for hyperpolarized ^{13}C imaging. *Magn Reson Med*. 2006;56(4):932-937. <https://doi.org/10.1002/mrm.21025>
42. Bilgic B, Gagoski B, Kok T, Adalsteinsson E. Lipid suppression in CSI with spatial priors and highly undersampled peripheral k -space. *Magn Reson Med*. 2013;69(6):1501-1511. <https://doi.org/10.1002/mrm.24399>
43. Hangel G, Strasser B, Považan M, et al. A comparison of lipid suppression by double inversion recovery, L1- and L2-regularisation for high resolution MRSI in the brain at 7 T. Paper presented at: *ISMRM 24th Annual Meeting & Exhibition*; May 7-13, 2016; Singapore.
44. Heckova E, Strasser B, Považan M, Hangel G, Trattng S, Bogner W. Absolute quantification of brain metabolites by 1H-MRSI using gradient echo imaging of $\sim 2\text{s}$ as a concentration reference: initial findings. Paper presented at: *ISMRM 25th Annual Meeting & Exhibition*; April 22-24, 2017; Honolulu, HI.
45. Provencher SW. Automatic quantitation of localized *in vivo* ^1H spectra with LCMoDel. *NMR Biomed*. 2001;14(4):260-264. <https://doi.org/10.1002/nbm.698>
46. Starčuk Z, Starčuková J, Štrbák O, Graveron-Demilly D. Simulation of coupled-spin systems in the steady-state free-precession acquisition mode for fast magnetic resonance (MR) spectroscopic imaging. *Meas Sci Technol*. 2009;20(10):104033. <https://doi.org/10.1088/0957-0233/20/10/104033>
47. Považan M, Strasser B, Hangel G, et al. Simultaneous mapping of metabolites and individual macromolecular components via ultra-short acquisition delay ^1H MRSI in the brain at 7T. *Magn Reson Med*. 2018;79(3):1231-1240. <https://doi.org/10.1002/mrm.26778>
48. Považan M, Hangel G, Strasser B, et al. Mapping of brain macromolecules and their use for spectral processing of ^1H -MRSI data with an ultra-short acquisition delay at 7 T. *NeuroImage*. 2015;121:126-135. <https://doi.org/10.1016/j.neuroimage.2015.07.042>
49. Harris AD, Puts NAJ, Edden RAE. Tissue correction for GABA-edited MRS: considerations of voxel composition, tissue segmentation, and tissue relaxations. *J Magn Reson Imaging*. 2015;42(5):1431-1440. <https://doi.org/10.1002/jmri.24903>

50. Xin L, Schaller B, Mlynarik V, Lu H, Gruetter R. Proton T_1 relaxation times of metabolites in human occipital white and gray matter at 7 T. *Magn Reson Med*. 2013;69(4):931-936. <https://doi.org/10.1002/mrm.24352>
51. Knight-Scott J, Brennan P, Palasis S, Zhong X. Effect of repetition time on metabolite quantification in the human brain in ^1H MR spectroscopy at 3 tesla. *J Magn Reson Imaging*. 2017;45(3):710-721. <https://doi.org/10.1002/jmri.25403>
52. Near J, Harris AD, Juchem C, et al. Preprocessing, analysis and quantification in single-voxel magnetic resonance spectroscopy: experts' consensus recommendations. *NMR Biomed*. 2021;34(5):e4257. <https://doi.org/10.1002/nbm.4257>
53. Gasparovic C, Song T, Devier D, et al. Use of tissue water as a concentration reference for proton spectroscopic imaging. *Magn Reson Med*. 2006;55(6):1219-1226. <https://doi.org/10.1002/mrm.20901>
54. Wilson M, Andronesi O, Barker PB, et al. Methodological consensus on clinical proton MRS of the brain: review and recommendations. *Magn Reson Med*. 2019;82(2):527-550. <https://doi.org/10.1002/mrm.27742>
55. Dale AM, Fischl B, Sereno MI. Cortical surface-based analysis. *NeuroImage*. 1999;9(2):179-194. <https://doi.org/10.1006/nimg.1998.0395>
56. Fischl B, Salat DH, Busa E, et al. Whole brain segmentation: automated labeling of neuroanatomical structures in the human brain. *Neuron*. 2002;33(3):341-355. [https://doi.org/10.1016/S0896-6273\(02\)00569-X](https://doi.org/10.1016/S0896-6273(02)00569-X)
57. Desikan RS, Ségonne F, Fischl B, et al. An automated labeling system for subdividing the human cerebral cortex on MRI scans into gyral based regions of interest. *NeuroImage*. 2006;31(3):968-980. <https://doi.org/10.1016/j.neuroimage.2006.01.021>
58. Spurny B, Heckova E, Seiger R, et al. Automated ROI-based labeling for multi-voxel magnetic resonance spectroscopy data using FreeSurfer. *Front Mol Neurosci*. 2019;12. <https://doi.org/10.3389/fnfmol.2019.00028>
59. de Graaf RA. *In Vivo NMR Spectroscopy*. Chichester, UK: Wiley; 2019 <https://doi.org/10.1002/9781119382461>
60. Zöllner HJ, Považan M, Hui SCN, Tapper S, Edden RAE, Oeltzschner G. Comparison of different linear-combination modeling algorithms for short-TE proton spectra. *NMR Biomed*. 2021;34(4):e4482. <https://doi.org/10.1002/nbm.4482>
61. Pouwels PJW, Frahm J. Differential distribution of NAA and NAAG in human brain as determined by quantitative localized proton MRS. *NMR Biomed*. 1997;10(2):73-78. [https://doi.org/10.1002/\(SICI\)1099-1492\(199704\)10:2<73::AID-NBM448>3.0.CO;2-4](https://doi.org/10.1002/(SICI)1099-1492(199704)10:2<73::AID-NBM448>3.0.CO;2-4)
62. Choi C, Coupland NJ, Bhardwaj PP, et al. T_2 measurement and quantification of glutamate in human brain in vivo. *Magn Reson Med*. 2006;56(5):971-977. <https://doi.org/10.1002/mrm.21055>
63. Gonen OM, Moffat BA, Desmond PM, Lui E, Kwan P, O'Brien TJ. Seven-tesla quantitative magnetic resonance spectroscopy of glutamate, γ -aminobutyric acid, and glutathione in the posterior cingulate cortex/precuneus in patients with epilepsy. *Epilepsia*. 2020;61(12):2785-2794. <https://doi.org/10.1111/epi.16731>
64. van Zijl PCM, Barker PB. Magnetic resonance spectroscopy and spectroscopic imaging for the study of brain metabolism. *Ann N Y Acad Sci*. 1997;820(1):75-96. <https://doi.org/10.1111/j.1749-6632.1997.tb46190.x>
65. Rai S, Chowdhury A, Reniers RLEP, Wood SJ, Lucas SJE, Aldred S. A pilot study to assess the effect of acute exercise on brain glutathione. *Free Radic Res*. 2018;52(1):57-69. <https://doi.org/10.1080/10715762.2017.1411594>
66. Terpstra M, Vaughan TJ, Ugurbil K, Lim KO, Schulz SC, Gruetter R. Validation of glutathione quantitation from STEAM spectra against edited ^1H NMR spectroscopy at 4T: application to schizophrenia. *Magn Reson Mater Phys Biol Med*. 2005;18(5):276-282. <https://doi.org/10.1007/s10334-005-0012-0>
67. Emir UE, Deelchand D, Henry P-G, Terpstra M. Noninvasive quantification of T_2 and concentrations of ascorbate and glutathione in the human brain from the same double-edited spectra. *NMR Biomed*. 2011;24(3):263-269. <https://doi.org/10.1002/nbm.1583>
68. van de Bank BL, Emir UE, Boer VO, et al. Multi-center reproducibility of neurochemical profiles in the human brain at 7 T. *NMR Biomed*. 2015;28(3):306-316. <https://doi.org/10.1002/nbm.3252>
69. Edden RAE, Pomper MG, Barker PB. In vivo differentiation of N-acetyl aspartyl glutamate from N-acetyl aspartate at 3 Tesla. *Magn Reson Med*. 2007;57(6):977-982. <https://doi.org/10.1002/mrm.21234>
70. Bhogal AA, Broeders TAA, Morsinkhof L, et al. Lipid-suppressed and tissue-fraction corrected metabolic distributions in human central brain structures using 2D ^1H magnetic resonance spectroscopic imaging at 7 T. *Brain Behav*. 2020;10(12):e01852. <https://doi.org/10.1002/brb3.1852>
71. Gambarota G, Meke R, Xin L, et al. In vivo measurement of glycine with short echo-time ^1H MRS in human brain at 7 T. *Magn Reson Mater Phys Biol Med*. 2009;22(1):1-4. <https://doi.org/10.1007/s10334-008-0152-0>
72. Choi C, Dimitrov I, Douglas D, et al. In vivo detection of serine in the human brain by proton magnetic resonance spectroscopy (^1H -MRS) at 7 Tesla. *Magn Reson Med*. 2009;62(4):1042-1046. <https://doi.org/10.1002/mrm.22079>
73. Zhang Y, Taub E, Mueller C, et al. Reproducibility of whole-brain temperature mapping and metabolite quantification using proton magnetic resonance spectroscopy. *NMR Biomed*. 2020;33(7):e4313. <https://doi.org/10.1002/nbm.4313>
74. Veenith TV, Mada M, Carter E, et al. Comparison of inter subject variability and reproducibility of whole brain proton spectroscopy. *PLoS ONE*. 2014;9(12):e115304. <https://doi.org/10.1371/journal.pone.0115304>
75. Roalf DR, Sydnor VJ, Woods M, et al. A quantitative meta-analysis of brain glutamate metabolites in aging. *Neurobiol Aging*. 2020;95:240-249. <https://doi.org/10.1016/j.neurobiolaging.2020.07.015>
76. Lind A, Boraxbekk C-J, Petersen ET, Paulson OB, Siebner HR, Marsman A. Regional myo-inositol, creatine, and choline levels are higher at older age and scale negatively with visuospatial working memory: a cross-sectional proton MR spectroscopy study at 7 Tesla on normal cognitive ageing. *J Neurosci*. 2020;40(42):8149-8159. <https://doi.org/10.1523/JNEUROSCI.2883-19.2020>
77. Chang L, Ernst T, Poland RE, Jenden DJ. In vivo proton magnetic resonance spectroscopy of the normal aging human brain. *Life Sci*. 1996;58(22):2049-2056. [https://doi.org/10.1016/0024-3205\(96\)00197-X](https://doi.org/10.1016/0024-3205(96)00197-X)
78. Endres D, Tebartz van Elst L, Feige B, et al. On the effect of sex on prefrontal and cerebellar neurometabolites in healthy adults: an MRS study. *Front Hum Neurosci*. 2016;10:367. <https://doi.org/10.3389/fnhum.2016.00367>
79. Hädel S, Wirth C, Rapp M, Gallinat J, Schubert F. Effects of age and sex on the concentrations of glutamate and glutamine in the human brain. *J Magn Reson Imaging*. 2013;38(6):1480-1487. <https://doi.org/10.1002/jmri.24123>
80. Gasparovic C, Chen H, Mullins PG. Errors in ^1H -MRS estimates of brain metabolite concentrations caused by failing to take into account tissue-specific signal relaxation. *NMR Biomed*. 2018;31(6):e3914. <https://doi.org/10.1002/nbm.3914>
81. Liao Y, Oros-Peusquens A-M, Lindemeyer J, et al. An MR technique for simultaneous quantitative imaging of water content, conductivity and susceptibility, with application to brain tumours using a 3T hybrid MR-PET scanner. *Sci Rep*. 2019;9(1):88. <https://doi.org/10.1038/s41598-018-36435-8>

82. Hernández-Tamames JA, Mato Abad V, García-Álvarez R, González-Zabaleta J, Pereira Loureiro J, Álvarez-Linera J. Effect of water T2 shortening in the quantification of in-vitro proton MR spectroscopy. *J Neuroimaging*. 2016;26(1):58-61. <https://doi.org/10.1111/jon.12258>
83. Hangel G, Strasser B, Považan M, et al. A comparison of lipid suppression by double inversion recovery, L1- and L2-regularisation for high-resolution MRSI in the brain at 7 T. Paper presented at: *ISMRM 24rd Annual Meeting & Exhibition*; May 7-13, 2016; Singapore.
84. Juchem C, Cudalbu C, Graaf RA, et al. B₀ shimming for in vivo magnetic resonance spectroscopy: experts' consensus recommendations. *NMR Biomed*. 2020;34(5):e4350. <https://doi.org/10.1002/nbm.4350>
85. Hetherington HP, Hamid H, Kulas J, et al. MRSI of the medial temporal lobe at 7 T in explosive blast mild traumatic brain injury. *Magn Reson Med*. 2014;71(4):1358-1367. <https://doi.org/10.1002/mrm.24814>
86. He X, Auerbach EJ, Garwood M, Kobayashi N, Wu X, Metzger GJ. Parallel transmit optimized 3D composite adiabatic spectral-spatial pulse for spectroscopy. *Magn Reson Med*. 2021;86(1):17-32. <https://doi.org/10.1002/mrm.28682>
87. Motyka S, Moser P, Hingerl L, et al. The influence of spatial resolution on the spectral quality and quantification accuracy of whole-brain MRSI at 1.5T, 3T, 7T, and 9.4T. *Magn Reson Med*. 2019;82(2):551-565. <https://doi.org/10.1002/mrm.27746>
88. Bogner W, Hess AT, Gagoski B, et al. Real-time motion- and B₀-correction for LASER-localized spiral-accelerated 3D-MRSI of the brain at 3T. *NeuroImage*. 2013;88C:22-31. <https://doi.org/10.1016/j.neuroimage.2013.09.034>
89. Andronesi OC, Bhattacharyya PK, Bogner W, et al. Motion correction methods for MRS localization and shimming: experts' recommendations. *NMR Biomed*. 2021;34(5). <https://doi.org/10.1002/nbm.4364>
90. Maudsley AA, Andronesi OC, Barker PB, et al. Advanced magnetic resonance spectroscopic neuroimaging: experts' consensus recommendations. *NMR Biomed*. 2021;34(5):e4309. <https://doi.org/10.1002/nbm.4309>
91. Kreis R, Boer V, Choi I-Y, et al. Terminology and concepts for the characterization of in vivo MR spectroscopy methods and MR spectra: background and experts' consensus recommendations. *NMR Biomed*. 2021;34(5). <https://doi.org/10.1002/nbm.4347>
92. Hangel G, Spurny B, Lazen P, et al. Supplementary MRSI data for "Inter-subject stability and regional concentration estimates of 3D-FID-MRSI in the human brain at 7T". 2021. <https://doi.org/10.5281/zenodo.5006923>
93. Lin A, Andronesi O, Bogner W, et al. Minimum reporting standards for in vivo magnetic resonance spectroscopy (MRSinMRS): experts' consensus recommendations. *NMR Biomed*. 2021;34(5):e4484. <https://doi.org/10.1002/nbm.4484>
94. An L, Araneta MF, Victorino M, Shen J. Determination of brain metabolite T₁ without interference from macromolecule relaxation. *J Magn Reson Imaging*. 2020;52(5):1352-1359. <https://doi.org/10.1002/jmri.27259>

SUPPORTING INFORMATION

Additional supporting information may be found online in the Supporting Information section at the end of this article.

How to cite this article: Hangel G, Spurny-Dworak B, Lazen P, et al. Inter-subject stability and regional concentration estimates of 3D-FID-MRSI in the human brain at 7 T. *NMR in Biomedicine*. 2021;34(12):e4596. <https://doi.org/10.1002/nbm.4596>